Impact of porosity and destructive effects on dust evolution using SPH simulations

Jean-François Gonzalez, Stéphane Michoulier

SF2A 2023
M. N'Diaye, A. Siebert, N. Lagarde, O. Venot, K. Baillié, M. Béthermin, E. Lagadec, J. Malzac, J. Richard (eds)

IMPACT OF POROSITY AND DESTRUCTIVE EFFECTS ON DUST EVOLUTION USING SPH SIMULATIONS

S. Michoulier[1] and J.-F. Gonzalez[1]

Abstract. In the theory of planetary formation, the process of how sub-µm to mm dust aggregates in protoplanetary discs grow into planetesimals is still poorly understood. A solution to overcome the fragmentation and radial drift barriers is to consider grain porosity (Garcia 2018). We have implemented a porosity evolution model in the SPH code Phantom based on Garcia (2018) and Garcia & Gonzalez (2020), with new destructive effects. With a disc model that reproduces observations, we show that porosity help grain growth as expected, allowing them to reach larger sizes. When fragmentation, bouncing and compaction are taken into account, it is still possible to form a thin disc of large dust in the mid-plane, with correct filling factors and sizes according to observations, something that can not be reproduced with compact grains.

Keywords: protoplanetary discs, planets and satellites: formation, methods: numerical

1 Introduction

Many ideas have been theorized to explain the formation of planets, yet none have been proven so far. Plenty of solutions have been proposed to form planets, mainly by forming dust traps via pressure maxima to create planetesimals, which are the building blocks of planet embryos. We can cite vortices (Barge & Sommeria 1995; Meheut et al. 2012), snow-lines (Kretke & Lin 2007; Vericel & Gonzalez 2020), or self-induced dust traps (Gonzalez et al. 2017; Vericel et al. 2021). Others classes of processes are based on instabilities, like the streaming instabilities (Youdin & Goodman 2005; Schäfer et al. 2017). Another solution is to consider more complex intrinsic properties of dust grains, namely their porosity. We have implemented a porosity evolution model that can be used in 3D simulations, developed by Garcia (2018) and Garcia & Gonzalez (2020), in the SPH code Phantom (Price et al. 2018). We also added new effects, mainly destructive, such as rotational disruption (Tatsuuma & Kataoka 2021; Michoulier & Gonzalez 2022), bouncing, and compaction during fragmentation. In this study, we will see how porosity and the different processes we added can affect the evolution of dust in discs compared to compact grains.

2 Models

2.1 Porosity and growth model

In order to take into account dust porosity, we use a slightly different and simplified version of the model derived by Garcia (2018) and Garcia & Gonzalez (2020), which contain all the details and equations about the evolution of porosity during growth. This model is based on the model from Suyama et al. (2008), Okuzumi et al. (2009), Okuzumi et al. (2012) and Kataoka et al. (2013). An aggregate is a collection of n monomers considered to be perfect compact spheres of mass m_0, size a_0 and intrinsic density ρ_s. The filling factor is defined as $\phi = \rho/\rho_\mathrm{s}$, i.e. the ratio between the aggregate's mean density and the intrinsic density of the monomers. The mass m, size s and mean density ρ of the grain can be computed as follows:

$$m = \rho V = \frac{4\pi}{3}\rho_\mathrm{s}\phi s^3. \tag{2.1}$$

[1] Universite Claude Bernard Lyon 1, CRAL UMR5574, ENS de Lyon, CNRS, Villeurbanne, F-69622, France

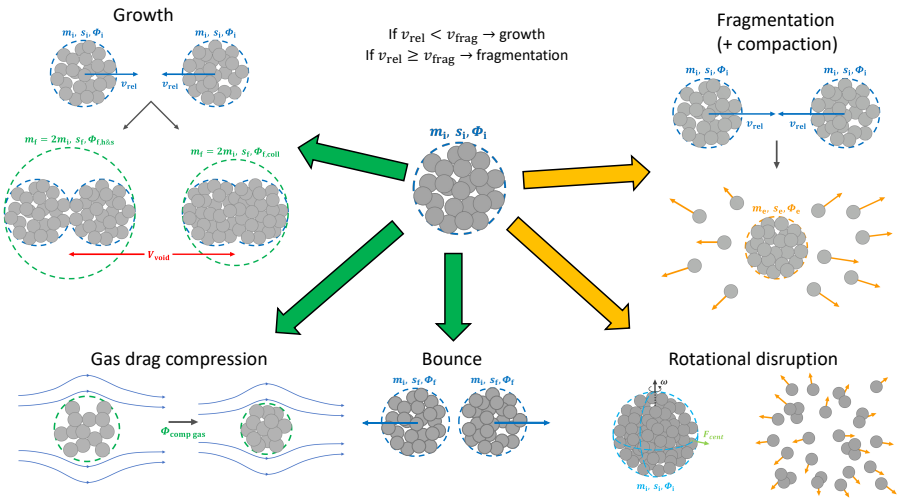

Fig. 1. Summary of some of the processes in our model a grain might undergo during its life. Some processes are destructive (yellow arrows), others lead to an increase or decrease of size, while the mass is conserved (green arrows).

The evolution of aggregates is driven by different regimes of expansion and compression depending on the mass of the grains. Grains can be in the "hit & stick" regime (see figure 1 left) or in collisional compression when masses increase. Independently of collisions, grains can also suffer static compaction (figure 1) due to gas flow (Kataoka et al. 2013). To model dust growth, we consider a locally uniform distribution of grain mass, where collisions occur between grains of identical mass m (Stepinski & Valageas 1996). Two grains collide with a relative velocity $v_{\rm rel}$ due to the gas turbulence transmitted to the dust by drag. This model was extensively used by Laibe et al. (2008), Gonzalez et al. (2015),Vericel et al. (2021). Moreover, grains can also bounce, when $\phi > 0.3$ (Wada et al. 2011; Shimaki & Arakawa 2012; Arakawa et al. 2023). Depending on $v_{\rm rel}$, the deformation can be elastic or plastic, the latter leading to compression. Some details on how bouncing is modeled are presented in Garcia (2018). The exact model will be presented in Michoulier & Gonzalez (in prep.).

2.2 Fragmentation, compaction and disruption

Lastly, to model fragmentation of dust aggregates, we use the model developed by Kobayashi & Tanaka (2010) and Garcia (2018), where the loss of mass is also a function of the fragmentation threshold $v_{\rm frag}$. The initial model supposes a constant filling during fragmentation. But Ringl et al. (2012) and Gunkelmann et al. (2016) have shown that the filling factor after fragmentation is approximately 1.5 to 2 times larger than the initial one. We have developed a model to take into account the compaction during fragmentation based on dust properties. The full model will also be presented in Michoulier & Gonzalez (in prep.). Finally, for the rotational disruption, we use the exact same model as the one detailed in Michoulier & Gonzalez (2022).

3 Results

For our simulations, we use the SPH code Phantom (Price et al. 2018) and the 1-fluid method. We use a disc model representative of observations (Williams & Best 2014). The mass of the star is set to $M_* = 1$ M$_\odot$, that of the disc to $M_* = 0.01$ M$_\odot$. The inner and outer radii are set to $r_{\rm in} = 10$ au and $r_{\rm out} = 400$ au, the disc aspect ratio is $H/r_0 = 0.0895$ with a reference radius $r_0 = 100$ au, $p = 0.75$, $q = 0.5$, and a turbulent viscosity parameter $\alpha = 5 \times 10^{-3}$. The external density profile decreases exponentially with a characteristic disc radius of $R_{\rm c} = 60$ au (see equation (298) in Price et al. 2018). For the dust, a typical dust-to-gas ratio of 1% is used. We use silicates with $\rho_{\rm s} = 2.7$ kg m^{-3}, a young modulus $\mathcal{E} = 72$ GPa (Yamamoto et al. 2014) and a surface energy of $\gamma_{\rm s} = 0.2$ J m^{-2} (Yamamoto et al. 2014; Kimura et al. 2020). The monomer size is fixed to 0.2 µm according to Tazaki & Dominik (2022), with different fragmentation thresholds $v_{\rm frag} = 5 - 10 - 20$ m s^{-1}.

Figures 2 and 3 show the results of six simulations at $t = 100$ kyr. GF-comp-Vf20 correspond to a simulation with growth and fragmentation with compact grains and $v_{\rm frag\,Si} = 20$ m s^{-1}, GF-a02-Vf20 is the same with porous grains with a monomer size of 0.2 µm. GBFc-a02-Vf10 and GBFc-a02-Vf20 correspond to simulations

with growth, fragmentation, bouncing and compaction and $v_{\mathrm{frag,\,Si}} = 10$ and 20 m s^{-1}. GBFcS-a02-Vf205 is GBFc-a02-Vf20 with a CO snow-line ($T = 20$ K) where $v_{\mathrm{frag,\,in}} = 20$ m s^{-1} and $v_{\mathrm{frag,\,out}} = 5$ m s^{-1} and GBFcD-a02-Vf20 is GBFc-a02-Vf20 with disruption. We can see on figure 2 showing the size s in the (r, z) plane that all cases produce thin discs in the inner regions, of the order of $15 - 20$ au thick at 100 au, except for GBFcS-a02-Vf205 where the disc is thicker due to the snow-line. We also note the outer region is thicker when porosity is taken into account. Large grains are located in the mid-plane, with sizes exceeding 100 µm. GF-a02-Vf20 and GBFc-a02-Vf20 are able to produce the largest grains, while GBFc-a02-Vf10 can't due to the lower fragmentation threshold that limit the grain size to 1 mm at maximum. Disruption (GBFcD-a02-Vf20) limits the maximum grain size compared to GBFc-a02-Vf20, as centimetre-sized aggregates are in this case harder to form. In the case of a snow-line, grains are not able to grow freely at distances larger than 100 au, where the CO snow-line is located, due to the very low v_{frag}. In the inner regions where v_{frag} is larger, dust grains larger than 1 mm are still formed with high filling factors. Figure 3 shows the radial size distribution colored with the

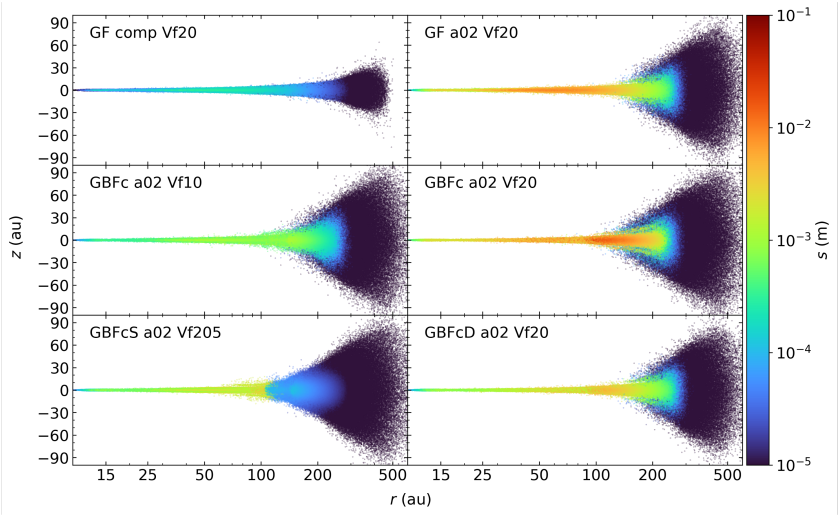

Fig. 2. Comparison between simulations in the (r, z) plane with growth and fragmentation with compact grains and $v_{\mathrm{frag\,Si}} = 20$ m s^{-1} (GF-comp-Vf20), the same with porous grains (GF-a02-Vf20), two simulations with growth, fragmentation, bouncing and compaction with $v_{\mathrm{frag,\,Si}} = 10$ and 20 m s^{-1} (GBFc-a02-Vf10 and GBFc-a02-Vf20). The last two are the same as GBFc-a02-Vf20. One with a CO snow-line (GBFcS-a02-Vf205) where $v_{\mathrm{frag,\,in}} = 20$ m s^{-1} and $v_{\mathrm{frag,\,out}} = 5$ m s^{-1}, the other one with disruption (GBFcD-a02-Vf20). The color gives the dust size.

filling factor ϕ. Simulation GF-comp-Vf20 with compact grains is not able to form grains of 1 mm anywhere in the disc. This is also the case of the simulation GBFc-a02-Vf10 where sizes of 1-2 mm are barely reached between 30 and 200 au. GF-a02-Vf20 and GBFc-a02-Vf20 are able to reach of a couple of centimetres in a large portion of the disc, even if GBFc-a02-Vf20 has compaction during fragmentation. The effect of disruption can be seen between 50 to 150 au where grains do not suffer from compaction. The maximum size is about 1 cm, while without disruption, the maximum is about 8 cm. Finally, the simulation with a snow-line shows compacted grains up to 100 au with $\phi \sim 0.1 - 0.5$ and $s \geq 1$mm, up to 1 cm at the snow-line at 100 au.

4 Conclusions

We have implemented a complete model of dust porosity evolution in Phantom. We performed several simulations with different processes to see their effect on dust evolution. When taking into account growth, fragmentation, bouncing and compaction (GBFc), simulations show it is possible to form grains with $\phi \sim 0.1 - 0.5$ and $s \sim 1$ mm, compatible with observations (Güttler et al. 2019; Guidi et al. 2022; Zhang et al. 2023). Bouncing is negligible and disruption does not play a huge role, as we excepted (Michoulier & Gonzalez 2022), while compaction during fragmentation is the mechanism that allows results closer to observations. Synthetic images are the next step to compare with observations and better understand how planets form.

We would like to thank the SF2A and the organizers of "Latest insights on dust evolution" for letting us present our work to the "Journées de la SF2A 2023". Figures in the results section were made using the *matplotlib* library (Hunter 2007).

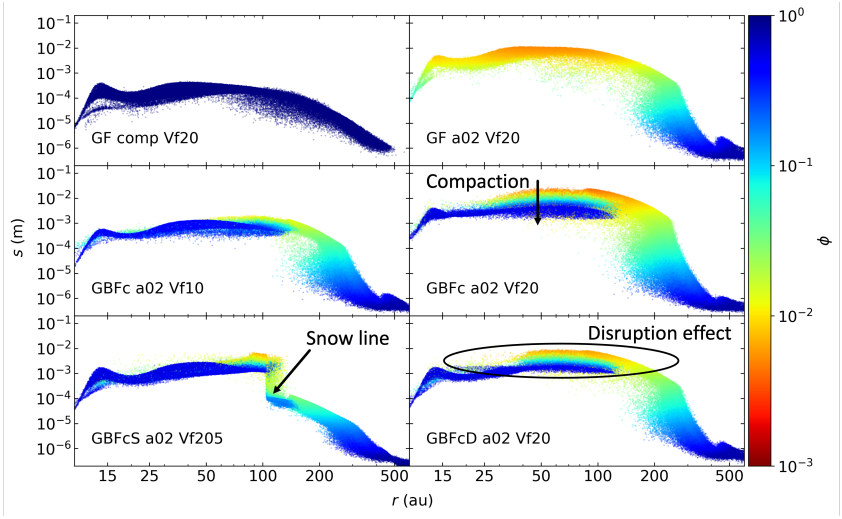

Fig. 3. Same as figure 2, but the grain size s is given as a function of r and color indicates the filling factor.

References

Arakawa, S., Okuzumi, S., Tatsuuma, M., et al. 2023, arXiv e-prints, arXiv:2306.04070
Barge, P. & Sommeria, J. 1995, A&A, 295, L1
Garcia, A. 2018, Theses, Université de Lyon
Garcia, A. J. L. & Gonzalez, J.-F. 2020, MNRAS, 493, 1788
Gonzalez, J.-F., Laibe, G., & Maddison, S. T. 2017, MNRAS, 467, 1984
Gonzalez, J.-F., Laibe, G., Maddison, S. T., Pinte, C., & Ménard, F. 2015, Planet. Space Sci., 116, 48
Guidi, G., Isella, A., Testi, L., et al. 2022, A&A, 664, A137
Gunkelmann, N., Ringl, C., & Urbassek, H. M. 2016, A&A, 589, A30
Güttler, C., Mannel, T., Rotundi, A., et al. 2019, A&A, 630, A24, arXiv: 1902.10634
Hunter, J. D. 2007, Computing in Science & Engineering, 9, 90
Kataoka, A., Tanaka, H., Okuzumi, S., & Wada, K. 2013, A&A, 557, L4
Kimura, H., Wada, K., Yoshida, F., et al. 2020, MNRAS, 496, 1667, arXiv: 2006.05107
Kobayashi, H. & Tanaka, H. 2010, Icarus, 206, 735
Kretke, K. A. & Lin, D. N. C. 2007, The Astrophysical Journal, 664, L55
Laibe, G., Gonzalez, J. F., Fouchet, L., & Maddison, S. T. 2008, A&A, 487, 265
Meheut, H., Keppens, R., Casse, F., & Benz, W. 2012, A&A, 542, A9
Michoulier, S. & Gonzalez, J.-F. 2022, MNRAS, 517, 3064
Okuzumi, S., Tanaka, H., Kobayashi, H., & Wada, K. 2012, ApJ, 752, 106
Okuzumi, S., Tanaka, H., & Sakagami, M.-a. 2009, ApJ, 707, 1247
Price, D. J., Wurster, J., Tricco, T. S., et al. 2018, Publications of the Astronomical Society of Australia, 35, e031
Ringl, C., Bringa, E. M., Bertoldi, D. S., & Urbassek, H. M. 2012, ApJ, 752, 151, aDS Bibcode: 2012ApJ...752..151R
Schäfer, U., Yang, C.-C., & Johansen, A. 2017, A&A, 597, A69
Shimaki, Y. & Arakawa, M. 2012, Icarus, 218, 737, aDS Bibcode: 2012Icar..218..737S
Stepinski, T. F. & Valageas, P. 1996, A&A, 309, 301
Suyama, T., Wada, K., & Tanaka, H. 2008, ApJ, 684, 1310
Tatsuuma, M. & Kataoka, A. 2021, ApJ, 913, 132
Tazaki, R. & Dominik, C. 2022, A&A, 663, A57
Vericel, A. & Gonzalez, J.-F. 2020, MNRAS, 492, 210
Vericel, A., Gonzalez, J.-F., Price, D. J., Laibe, G., & Pinte, C. 2021, MNRAS, 507, 2318
Wada, K., Tanaka, H., Suyama, T., Kimura, H., & Yamamoto, T. 2011, ApJ, 737, 36
Williams, J. P. & Best, W. M. J. 2014, ApJ, 788, 59, aDS Bibcode: 2014ApJ...788...59W
Yamamoto, T., Kadono, T., & Wada, K. 2014, ApJ, 783, L36
Youdin, A. N. & Goodman, J. 2005, ApJ, 620, 459, aDS Bibcode: 2005ApJ...620..459Y
Zhang, S., Zhu, Z., Ueda, T., et al. 2023, arXiv e-prints, arXiv:2306.00158